RSC Advances

PAPER

View Article Online
View Journal | View Issue

Cite this: *RSC Adv.*, 2018, **8**, 40369

Silica modification of titania nanoparticles enhances photocatalytic production of reactive oxygen species without increasing toxicity potential *in vitro*

Simona Ortelli,[a] Anna L. Costa,*[a] Pietro Matteucci,[b] Mark R. Miller,[c] Magda Blosi,[a] Davide Gardini,[a] Syed A. M. Tofail,[d] Lang Tran,[e] Domenica Tonelli[b] and Craig A. Poland[c]

Titania (TiO_2) nanoparticles were surface modified using silica and citrate to implement a 'safe-by-design' approach for managing potential toxicity of titania nanoparticles by controlling surface redox reactivity. DLS and zeta-potential analyses confirmed the surface modification, and electron microscopy and surface area measurements demonstrated nanoscale dimensions of the particles. Electron paramagnetic resonance (EPR) was used to determine the exogenous generation of reactive oxygen species (ROS). All the produced spray dried nanotitania lowered levels of ROS when compared to the corresponding dispersed nanotitania, suggesting that the spray drying process is an appropriate design strategy for the control of nano TiO_2 ROS reactivity. The modification of nanotitania with silica and with citrate resulted in increased levels of ROS generation in exogenous measurements, including photoexcitation for 60 minutes. The dichlorodihydrofluorescein (DCFH) assay of dose-dependent production of oxidative stress, generated by pristine and modified nanotitania in macrophages and alveolar epithelial cells, found no significant change in toxicity originating from the generation of reactive oxygen species. Our findings show that there is no direct correlation between the photocatalytic activity of nanotitania and its oxidative stress-mediated potential toxicity, and it is possible to improve the former, for example adding silica as a modifying agent, without altering the cell redox equilibrium.

Received 4th September 2018
Accepted 12th November 2018

DOI: 10.1039/c8ra07374k

rsc.li/rsc-advances

Introduction

In recent years, the presence of nanomaterials (NMs) in biological systems (bio-accessibility or bioavailability) has risen due to the increasing use of these NMs in a large number of advanced applications as a key to industrial innovation. There is also the potential for many of these NMs to produce detrimental effects on human health and the environment. This necessitates paying close attention to safety issues pertaining to NMs and their further development. Nanoparticles (NPs) can exert toxicity through oxidative stress, inflammation, genetic damage, inhibition of cell division and cell death.[1–4] For example, photocatalytic NPs of semiconducting oxides, such as titanium dioxide (TiO_2) and zinc oxide (ZnO), have found extensive use in applications prohibiting cellular growth and enabling self-sterilization.[5] The challenge in the field of using photocatalytic particles remains in finding appropriate conditions, *e.g.*, the amount of local surface charge that will initiate a desired, or inhibit an undesired biological action.[6] The above holds true for metal oxide NPs which have widespread use in industry for numerous applications ranging from sunscreens, pigments and construction materials for solar cells.[7–11]

Evidence is abundant within the literature that changes in structural and physicochemical properties of NPs can modify their biological activities, especially in relation to exogenous and endogenous generation of reactive oxygen species (ROS), one of the most frequently reported NP-associated toxicity mechanism.[2,12] Relatively rare is the endeavour in using these changes as a means to design NMs that would manage the safety concern of these NPs.[13] Reactive oxygen species are known to be able to cause oxidative damages to key structures and components of cells including DNA, proteins and lipids thus leading to significant functional changes of the cell as well as a disruption of cell

[a]*CNR-ISTEC, Institute of Science and Technology for Ceramics – National Research Council of Italy, Via Granarolo 64, I-48018 Faenza, RA, Italy. E-mail: anna.costa@istec.cnr.it*

[b]*Department of Industrial Chemistry, University of Bologna, Viale del Risorgimento 4, 40136 Bologna, Italy*

[c]*Queen's Medical Research Institute, University of Edinburgh, Edinburgh EH16 4TJ, UK*

[d]*Department of Physics, Bernal Institute, University of Limerick, V94 T9PX, Ireland*

[e]*Institute of Occupational Medicine, Research Avenue North, Riccarton, Edinburgh EH14 4AP, UK*

signalling, induction of inflammatory pathways, apoptosis and cell death.[14] Many studies have found that such oxidative stress is a prominent feature of the cellular response to TiO_2 NPs,[15] particularly when illuminated with ultraviolet (UV) light.[16,17] A direct, quantitative, correlation between extracellular and cellular pro-oxidant responses is highly desired, but currently lacking,[18] due to the sheer extent of the physicochemical properties of NM (*e.g.* size, shape, structure, and chemistry of the core and the coating/shell) that can impact biological effects such as toxicity within a complex biological matrix.

Despite the limited knowledge of such a correlation, surface modification of NPs has emerged as a potential method to implement a "Safe-by-Design" (SbD) approach to minimise unwanted biological activity such as NP toxicity. This approach can be a vital tool in the governance of nano-safety. Examples of modification strategies include silica coating of potentially toxic NPs due to the chemical inertia,[19] biocompatibility[20] and low toxicity[21] of silica as well as its ability to create mesoporous structure[22] and control ROS production.[23] In addition, citrate coating has been used as an organic coating strategy, due to the hydrophilicity and negative surface charge of citrates, that leads to an increased ability of dispersing NPs in an aqueous medium, a strong specific interaction with the hydroxyl groups in NPs, and an electrostatic hindrance to the contact of NPs with negatively charged cellular membrane.[24–26]

The quantitative determination of the impact of such modifications of physicochemical properties by SbD approach on functional properties is important in forecasting potential biological responses using established *in vitro* toxicity models.[27] The generation of ROS by engineered NPs can be determined either by exogenous, acellular factors or endogenous factors. Exogenous factors include intrinsic reactivity of NPs depending on structural characteristics as well as composition, activation by UV light, and/or a presence of metal impurities on the surface. On the other hand, endogenous factors include the ability to interfere with cellular redox machinery so inducing an excess of ROS production by target and inflammatory cells, processes in which mitochondrial respiration and activation of NAD(P)H-like enzyme systems are thought to be involved.[28,29]

In the present work, we use the exogenous approach to obtain a quantitative insight into the implementation of SbD approach in managing ROS production by titania NPs to induce cellular oxidative stress. The propensity of different modified TiO_2 to produce ROS in abiotic condition is evaluated through electron paramagnetic resonance (EPR) analysis using Tempone-H as the spin trap molecule. EPR provides a sensitive and relatively high-throughput means to test a panel of modified TiO_2 for photocatalytic ROS production. Findings from EPR were compared with that of the cellular dichlorodihydrofluorescein diacetate (DCFH-DA) assay for oxidative stress without any photoexcitation as it would be normal in an *in vivo* condition without any internal photoexcitation source. Both macrophages and epithelial cells were used for *in vitro* identification of the main predictors (colloidal/structural properties, spin-trapped ROS) which best describe the cellular response.

Results and discussion

Characterisation of colloidal nanosols

The optimal conditions for the self-assembled hetero-coagulation process between different colloidal phases occur when such species exhibit, at the working pH, ζ potentials opposite in sign and high enough to preserve colloidal stabilization and avoid homocoagulation. These conditions are fulfilled at pHs lower than the isoelectric point of TiO_2 (pH 7.1), where TiO_2 and SiO_2 present positive and negative ζ potentials, respectively (Table 1, Fig. 1). SiO_2 colloidal stabilization was decreased at pH 4.0, promoting the silica coagulation over nanotitania surface. The increase of the hydrodynamic diameter with the progressive addition of SiO_2 (Table 1) is caused both by the steric hindrance due to SiO_2 particles hetero-coagulated on the TiO_2 surface[40,41] and by the electrostatic destabilization induced by the neutralization of TiO_2 positive-charged surface with the SiO_2 negative charged particles. Since the ζ potential of the nanocolloidal systems is strictly linked to their agglomeration grade[30] the relationship between particle size and the predicted surface charge is complex. However, a decreasing ζ potential was observed for higher amounts of SiO_2, and the failure to achieve negative ζ potential for TiO_2 : SiO_2_1 : 3_COL and TiO_2 : SiO_2_1 : 5_COL samples suggested the formation of TiO_2/SiO_2 matrix encapsulation structures,[42] despite a typical core–shell structure, which were confirmed by STEM (Fig. 2c). In fact, TiO_2 : SiO_2_1 : 5_COL exhibited a random distribution of small TiO_2 nanoparticles

Table 1 Physicochemical characteristics of TiO_2/SiO_2nanosol samples[a]

Sample	pH	d_{DLS} (nm)	ζ potential (mV)	$pH_{i.e.p.}$
TiO_2_COL	2.8	53 ± 0.9	+38 ± 1.8	7.1
TiO_2 : SiO_2_1 : 3_COL	3.1	110 ± 0.9	+31 ± 1.0	6.0
TiO_2 : SiO_2_1 : 5_COL	3.4	577 ± 39	+25 ± 0.1	5.4
TiO_2 : CIT_1 : 0.8_COL	6.0	64 ± 0.9	−38 ± 1.9	nd
SiO_2_COL	9.6	20 ± 0.3	−42 ± 2.2	<3

[a] nd: not determined.

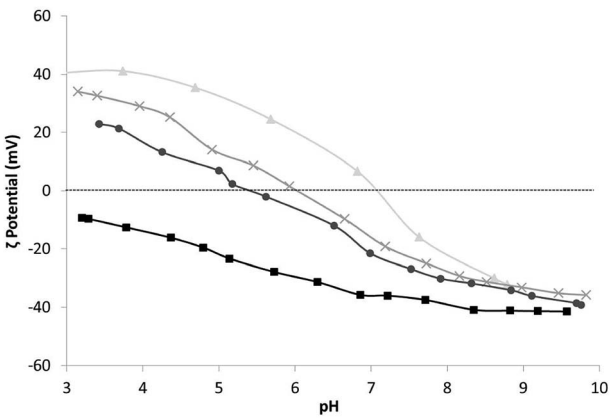

Fig. 1 ζ potential *vs.* pH of samples: ▲ TiO_2_COL, × TiO_2 : SiO_2_1-: 3_COL, ● TiO_2 : SiO_2_1 : 5_COL and ■ SiO_2_COL.

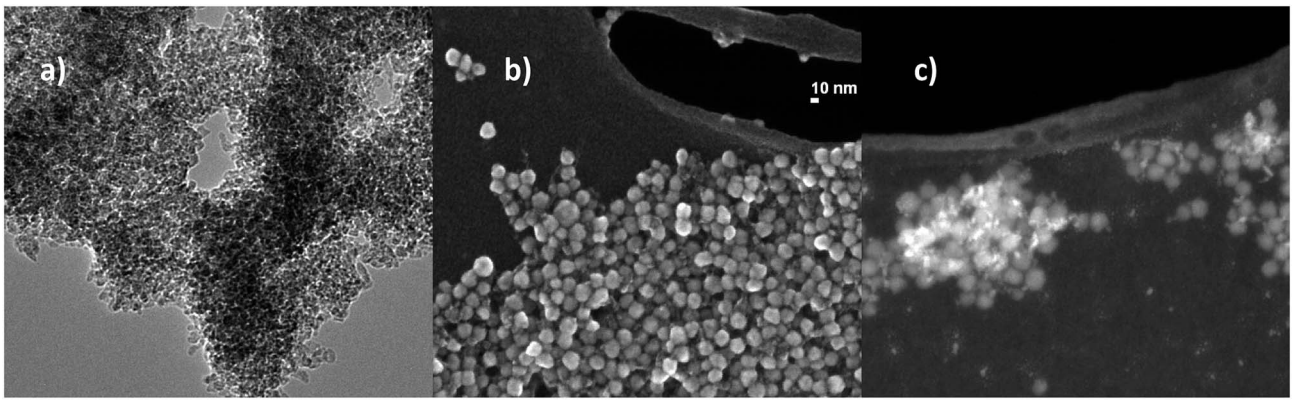

Fig. 2 Representative electron microscopy images of nanosol samples. (a) TEM image TiO_2_COL particles, (b) STEM and (c) STEM-HAADF image of TiO_2 : SiO_2_1 : 5_COL particles.

Table 2 Physicochemical characteristics of TiO_2/SiO_2 spray-dried samples

Sample	SA_{BET} (m^2 g^{-1})	ζ potential (mV)
TiO_2_SD	154	+43 ± 0.8
TiO_2 : SiO_2_1 : 3_SD	156	+22 ± 0.3
TiO_2 : SiO_2_1 : 5_SD	175	−15 ± 1.2
SiO_2_SD	174	−34 ± 0.9

(~5 nm, in the specific 4.82 ± 0.74 nm) within a silica matrix composed by particles of about 20 nm (18.98 ± 1.47 nm) of overall diameter (Fig. 2b). The pristine sample, TiO_2_COL, (Fig. 2a) was confirmed to have a diameter of ~5 nm for the primary particles, which appear clearly agglomerated, as a consequence of the sample preparation process for the microscope analysis.

The citrate added to the sample TiO_2 : CIT_1 : 0.8_COL acted as dispersant/capping agent, without any change in hydrodynamic diameter or colloidal stability over time, compared to the pristine titania. The negative ζ potential assessed for this sample (−38 mV) is consistent with the formation of a uniform negatively-charged citrate coating around TiO_2 nanoparticles.

Characterisation of spray-dried powders

SEM images of the particles prepared from the commercial titania nanosol (TiO_2_COL) pointed out dimensions in the range of 1–15 micrometres, with irregular surface hollows, as typical of spray dried particles derived from suspensions containing salts[43] (Fig. 5a). Despite the micrometric size, the assessed surface area is of 154 m^2 g^{-1} (Table 2), suggesting that the surface of the micrometric particles is actually nanostructured due to the collapsed nanoparticles contained in the starting nanosol.

The nanostructured surface, as demonstrated by a high BET value and SEM analysis (Fig. 3e), was clearly verified for all the

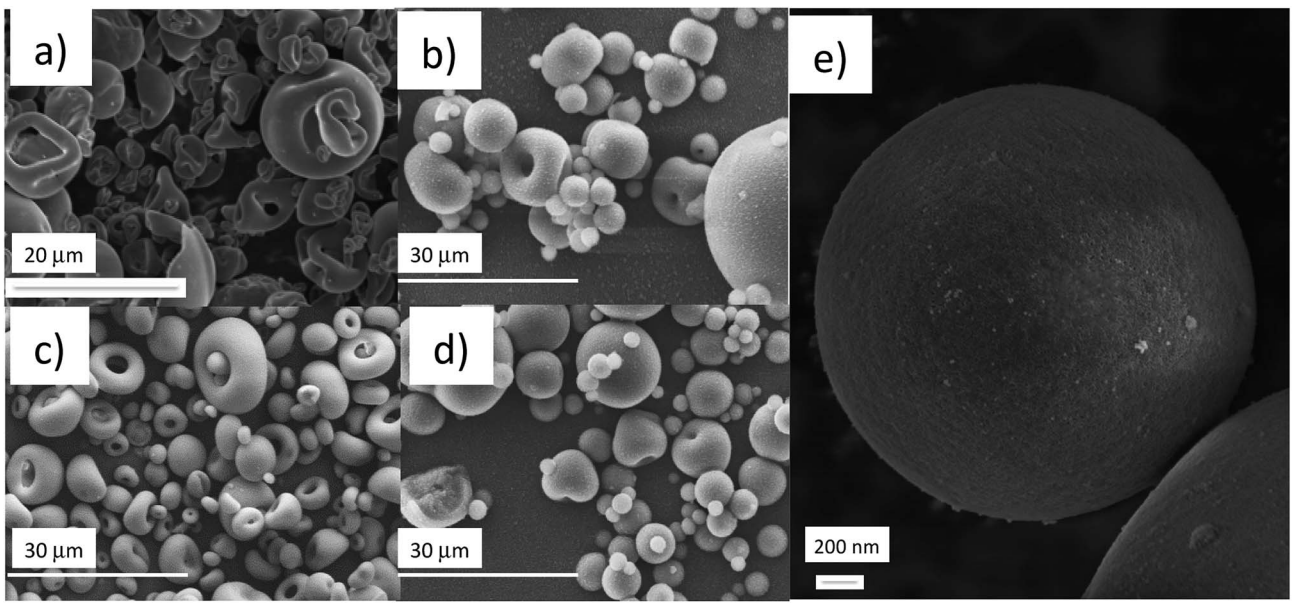

Fig. 3 SEM images of spray-dried powders from (a) TiO_2_SD, (b) TiO_2 : SiO_2_1 : 3_SD, (c) TiO_2 : SiO_2_1 : 5_SD, (d) SiO_2_SD and (e) high magnification of the surface of TiO_2 : SiO_2_1 : 5_SD.

spray dried samples. Some differences in the particle shapes were observed for increasing SiO_2 contents. For example, the spray-dried sample SiO_2_SD, obtained from the sol containing SiO_2 only, was micrometric in size with high specific surface area (174 m^2 g^{-1}) (Table 2), but with a highly regular and spherical or 'donut' shape (Fig. 3d). The spray dried powders TiO_2 : SiO_2_1 : 3_SD and TiO_2 : SiO_2_1 : 5_SD displaying different SiO_2 : TiO_2 ratios (3 and 5 : 1, respectively) exhibited a progressive regular morphology (Fig. 3b and c) with SiO_2 increasing, with a size from 2–20 micrometres and high BET specific surface areas of 156 and 175 m^2 g (Table 2).

ζ potential measurements performed after spray drying confirmed both for TiO_2 SD and for TiO_2 : SiO_2_1 : 3_SD positive values, as already assessed on the heterocoagulated suspension form (Table 2). However, the spray dried sample with a large excess of SiO_2 (TiO_2 : SiO_2_1 : 5_SD) had a negative ζ potential (Table 2), *i.e.*, a charge inversion with respect to the corresponding sample before spray drying, TiO_2 : SiO_2_1 : 5_COL. This behaviour is consistent with the presence of a more uniform and shielding SiO_2 coating formed on the TiO_2 surface during heat drying step.

ROS detection from acellular system by EPR measurements

EPR experiments with different concentrations and UV irradiation times showed a linear correlation between EPR intensity and UV irradiation time. Due to the linearity, using an irradiation time of 60 minutes the optimal EPR signal, was provided and used to compare the different NPs. The SiO_2 samples (SiO_2_COL and SiO_2_SD) did not generate any ROS species under UV irradiation.

In colloidal samples, after normalization in TiO_2 content, the silica doped surfaces led to greater values of ROS even though SiO_2 alone is not photoactive during UV irradiation (Fig. 4). Similarly, a slight ROS production increase if compared to pristine TiO_2 (TiO_2_COL), was observed in citrate-modified sample (TiO_2 : CIT_1 : 0.8_COL). Moreover, among all the samples, the colloidal sols had a greater reactivity and were more photoactive than the spray-dried powders (Fig. 4). The last observation is not surprising, if considering the decrease of free, available, surface reactive sites when passing from the dispersed nano particles to the agglomerated structures of granulated spray-dried micro particles.

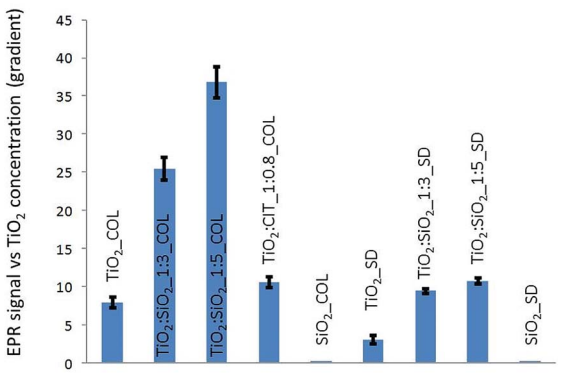

Fig. 4 ROS production estimated by the line slope of EPR signal intensity as a function of TiO_2 concentration.

In assessing the impact of UV irradiation of coated and uncoated TiO_2, analysing the data in Fig. 4, the silica coating appears to cause an enhancement of ROS production, despite silica is not able to produce oxygen radicals on its own. This behaviour could be ascribed to the potential ability of silica to prevent the radical recombination through the formation of hydrogen peroxide molecules, as elsewhere reported.[44] Photoabsorption in TiO_2 produces, in fact, conduction band electrons (e^-) and valence band holes (h^+) (eqn (1)). The quantity of H_2O_2 produced by the chain reactions comes from both the reduction of the oxygen molecules by the conduction band electrons (eqn (2) and (3)) and by water oxidation by the valence band holes (eqn (4) and (5)).

$$TiO_2 + h^+ \rightarrow TiO_2\,(e^- + h^+) \quad (1)$$

$$e^- + O_2 \rightarrow \cdot O_2^- \quad (2)$$

$$\cdot O_2^- + e^- + 2H^+ \rightarrow H_2O_2 \quad (3)$$

$$H_2O_2 + e^- \rightarrow \cdot OH + OH^- \quad (3')$$

$$h^+ + H_2O \rightarrow \cdot OH + H^+ \quad (4)$$

$$\cdot OH + h^+ + H_2O \rightarrow H_2O_2 + H^+ \quad (5)$$

The authors hypothesized that silica coating decreased the H_2O_2 formation, possibly through inhibition of the reactions (3) and (5), thus increasing the availability of intermediate radicals, $O_2^{\cdot -}$ and ·OH, as detected by EPR in the present study.

Cellular oxidative stress

The potential of pristine and modified NPs to induce oxidative stress in cells was assessed using the DCFH-DA assay in both macrophage (RAW 264.7) and epithelial cell (A549) lines (Fig. 5 and 6). In macrophages the pristine material (TiO_2_COL) dose dependently increased DCFH oxidation. However, due to the variations in the amplitude of the response the results were not statistically significant from control. In contrast, TiO_2 : SiO_2_1 : 3_SD dose dependently and significantly induced oxidative stress in macrophages, and the effect was statistically significant at the highest dose tested (40 μg cm^{-2}). None of the other tested NPs induced significant levels of DCFH oxidation in macrophages. The benchmark material P25 TiO_2 slightly increased the level of oxidative stress in macrophages (up to 1.2-fold), however, the results were not statistically significant compared to the control (Fig. 5).

In alveolar epithelial cells (Fig. 6), none of the tested compounds dose-dependently changed the degree of DCFH oxidation in a significant way. Importantly, TiO_2 : SiO_2_1 : 3_SD increased the levels of ROS in alveolar epithelial cells, as seen in macrophages, but the results did not reach statistical significance (at 40 μg cm^{-2}).

In colloidal nanosols, the presence of silica gave indications of oxidative stress, albeit modestly. In contrast, for spray-dried samples, the presence of silica slightly increased the oxidative stress, with the highest activity again shown by TiO_2 : SiO_2_1-: 3_SD sample. However, a dose dependent trend in oxidative

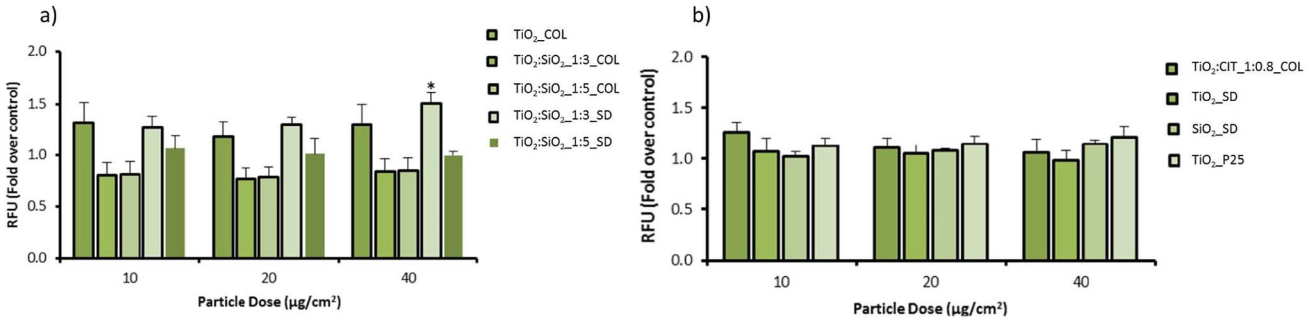

Fig. 5 The effect of NPs on oxidative stress in macrophages. Cells were treated for 24 hours with or without the various particles at different concentrations. Oxidative stress was analysed by incubating cells with the DCFH-DA. Results are expressed as fold change in fluorescence compared to the control +/− sem ($n = 3$).

stress in response to silica content or in the presence of citrate as surface modifier was not observed (Fig. 5 and 6).

The effects of P25 TiO_2 on oxidative stress, as assessed by the DCFH assay, have been reported in the literature. However, contradictory findings are frequent, demonstrating the difficulty to determine specific reactivity inherent to ROS and oxidative stress in nano-sized samples, especially due to the lack of consistency between experimental conditions and time points. For example, Kroll *et al.* showed that P25 TiO_2 induced oxidative stress to some extent in four different cell lines after 1 h incubation, but they did not find evidence of any effect either in macrophages or in alveolar epithelial cells.[45]

In macrophages, Kang *et al.* showed that a 4 hour incubation of 0.5 to 100 μg mL^{-1} P25 TiO_2 induced oxidative stress, yet by 24 hours, oxidative stress was evident only for 5 and 25 μg mL^{-1} P25 TiO_2. The authors also used fluorescent microscopy with another probe, dihydroethidium, demonstrating oxidative stress in macrophages treated with P25 TiO_2 for 30 minutes.[46] Contrary to the findings of Kroll *et al.*[45] using alveolar epithelial cells, signs of oxidative stress have been reported[47] following incubation for 1 h with P25 TiO_2 1.5 μg cm^{-2}. Other studies using alveolar epithelial cells have shown induction of oxidative stress following incubation with P25 TiO_2 at 2 h and 24 h, however the doses used were not directly comparable.[48] Here, amorphous silica on its own did not induce any form of oxidative stress in alveolar epithelial cells and macrophages. In macrophages, Yang *et al.* showed that 20 nm silica nanoparticles induced oxidative stress at concentrations higher than those tested in the present study.[49] Sohaebuddin *et al.*[50] showed that 30 nm SiO_2 nanoparticles induced oxidative stress in macrophages after 2 h incubation at 100 μg mL^{-1}. Others found out that SiO_2 nanoparticles dose dependently induced oxidative stress after longer periods of incubation (48–72 h) in alveolar epithelial cells.[51,52] In some cases, these results were gathered from longer incubation time using particles concentrations higher than 40 μg cm^{-2}, the highest dose of the present study.

Experimental

Materials

The following commercial products were used for the preparation of TiO_2/SiO_2 samples: TiO_2 colloidal nano-suspension ("TiO_2_COL") containing 6 wt% TiO_2, (anatase 84%, brookite 16%)[30] was provided by Colorobbia, Italy and SiO_2 colloidal nano-suspension ("SiO_2_COL") Ludox HS-40® containing 40 wt% SiO_2 by Grace Davison, USA. The nanopowder AEROXIDE® TiO_2 P25 (anatase 83% rutile 17%)[31] was used as reference material. Tempone-H hydrochloride (1-hydroxyl-2,2,6,6-tetramethyl-4-oxo-piperidine·HCl) was purchased from Enzo Life Sciences (Exeter, UK).

Preparation of modified TiO_2 samples

The commercial colloidal nano-suspensions (nanosols) were diluted with deionised water (TiO_2 and SiO_2 nanosols to 3 wt%) and, in the case of SiO_2 nanosol, acidified by cationic

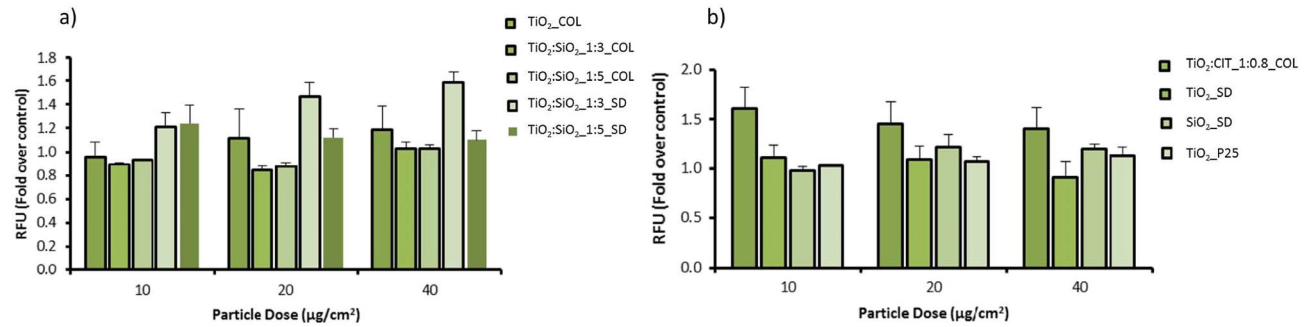

Fig. 6 Oxidative stress analysis in alveolar epithelial cells. Cells were treated for 24 hours with or without the various particles at different concentrations. Oxidative stress was analysed by incubating cells with the DCFH-DA probe. Results are expressed as fold change in fluorescence compared to the control +/− sem ($n = 3$).

exchange on resin at pH 4. Titania and silica nanosols were then mixed in defined ratios (TiO_2 : SiO_2 weight ratios 1 : 3 and 1 : 5) and ball-milled for 24 hours with 5 mm diameter zirconia spheres as milling media in order to form silica modified "TiO_2 : SiO_2_1 : 3_COL" and "TiO_2 : SiO_2_1 : 5_COL" samples through a self-assembled heterocoagulation process. In order to increase the adhesion of silica NPs to the surfaces of TiO_2 NPs, the heterocoagulated nanosols were spray-dried in counterflow with a stream of hot air (220 °C) through a nozzle of 500 μm of diameter (Fig. 7) to obtain spray-dried powder with TiO_2 : SiO_2 weight ratios 1 : 3 and 1 : 5 ("TiO_2 : SiO_2_1 : 3_SD" and "TiO_2 : SiO_2_1 : 5_SD", respectively). Pristine nanosols: TiO_2 and SiO_2 were also spray-dried, ("TiO_2_SD" and "SiO_2_SD").

Organic modification was achieved through citrate coating. The sample was prepared adding trisodium citrate dihydrate (Cit) to TiO_2_COL with TiO_2 : Cit weight ratio 1 : 0.8, with a TiO_2 concentration of 3 wt% *via* self-assembled monolayer formation[32] obtaining "TiO_2 : CIT_1 : 0.8_COL" sample. The mechanical stirring process was continued for 15 h to promote the re-dispersion of TiO_2 NPs.

Characterisation of colloidal nanosols

Hydrodynamic diameter and ζ potential of tested NPs (1 g L^{-1} in deionized water) were evaluated with a Zetasizer Nano ZSP (model ZEN5600, Malvern Instruments, UK). Hydrodynamic diameters obtained from dynamic light scattering (DLS) data (d_{DLS}) were derived from a measurement angle of 173° and automatic measurement duration. After 2 min temperature equilibration step (25 °C), 1 mL of sample volume was subjected to three consecutive measurements and particle size distribution by intensity was obtained by averaging these measurements. ζ potential measurements were performed on 700 μL sample at 25 °C by Electrophoretic Light Scattering (ELS) technique. Smoluchowski equation was applied to convert the electrophoretic mobility to ζ potential. After a 2 min temperature equilibration step, the samples underwent three measurements and ζ potential value was obtained by averaging these measurements. ζ potential of nanosols as a function of pH, was derived from Zetasizer Nano ZSP equipped with an automatic titrating system, by addition of 0.1 M KOH solution to TiO_2 based nanosols and 0.1 M HCl to SiO_2 nanosol (experimental uncertainty: 1 mV for ζ potential and 0.2 for pH). The ζ potential *vs.* pH titrations allowed identification of the isoelectric point (i.e.p.); the pH at which ζ potential sets to zero (pH i.e.p.). Morphological analysis was carried out by transmission electron microscopy (TEM) using a JEOL JEM-2100F multipurpose, high resolution, electron microscope with a field emission source operating between 80–200 kV. The nanoparticles were taken directly from the sols, placed on holey carbon grids for TEM analysis and air-dried at room temperature in a sealed environment for 2 hours.

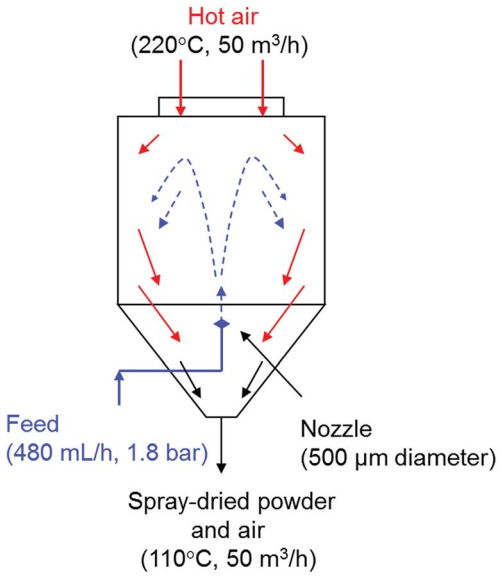

Fig. 7 Spray-drying technique applied to heterocoagulated nanosols.

Characterisation of spray-dried powders

The powder morphology was analysed using a scanning electron microscope (Leica, Cambridge Stereoscan 360, UK). Samples were prepared by placing powders on graphite double-sided adhesive into the aluminium stub. Surface area of spray-dried powders was measured by nitrogen adsorption (BET) (Sorpty 1750, Carlo Erba).

EPR analysis

Preparation of nano-TiO_2 based suspensions. Samples were suspended in a buffered physiological saline solution (PSS; composition: 118.4 mM NaCl, 25 mM $NaHCO_3$, 11 mM glucose, 4.7 mM KCl, 1.2 mM $MgSO_4$, 1.2 mM KH_2PO_4 and 2.5 mM $CaCl_2$, pH 7.4), in order to simulate the physiological and biological environment, and the measurements were performed at the same pH value.[33] For all the samples, the buffer solution was diluted 1 : 100, in order to avoid a destabilization of NP dispersion due to the electrostatic double layer compression. All the suspensions were dispersed by sonication bath (US 70; Philip Harris Scientific, Lichfield, UK) for 15 min, at room temperature. The following suspensions at concentrations of: 200, 300, 500, 1000, 2000, 3000 and 5000 μg mL^{-1}, starting from a stock suspension of 10 mg L^{-1}, were tested in order to obtain an analytical signal significantly different from the blank one. The analysed samples are reported in Table 3.

Table 3 Samples analysed by EPR spectroscopy[a]

Sample name	Physical form	Chemical composition	pH
TiO_2_SD	Spray-dried	TiO_2	nd
SiO_2_SD	Spray-dried	SiO_2	nd
TiO_2 : SiO_2_1 : 5_SD	Spray-dried	TiO_2 : SiO_2 = 1 : 5	nd
TiO_2 : SiO_2_1 : 3_SD	Spray-dried	TiO_2 : SiO_2 = 1 : 3	nd
TiO_2_COL	Colloidal	TiO_2	1.6
SiO_2_COL	Colloidal	SiO_2	4.1
TiO_2 : SiO_2_1 : 5_COL	Colloidal	TiO_2 : SiO_2 = 1 : 5	2.0
TiO_2 : SiO_2_1 : 3_COL	Colloidal	TiO_2 : SiO_2 = 1 : 3	1.9
TiO_2 : CIT_1 : 0.8_COL	Colloidal	TiO_2 : citrate = 1 : 0.8	4.9

[a] nd: not determined.

EPR spectroscopy with Tempone-H hydrochloride. Tempone-H hydrochloride (1-hydroxyl-2,2,6,6-tetramethyl-4-oxo-piperidine·HCl)[34] (Fig. 8a) was used as spin-trap molecule to create very stable radicals in aqueous solution for quantification during the time analyses. Tempone-H has preferential selectivity towards superoxide radicals ($O_2^{\bullet -}$) and hydroxyl radicals ($OH^{\bullet}$), with greater sensitivity than many conventional spin-traps (*e.g.* DMPO).[35,36] The spin-trap was dissolved in a 0.01 M EDTA (final concentration 0.1 mM) to minimize metal-ion-induced autoxidation.

Pyrogallol (320 μM in physiological saline solution) was used as positive control to assess the generation of superoxide radicals during the time analysis.[37] Samples were kept at 37 °C (in order to simulate body temperature) and the measurements taken by withdrawing a 50 μL sample into a capillary tube (Scientific Laboratory Ltd., Coatbridge, UK) plugged with Cristaseal (VWR International, Lutterwoth, UK). The intensity of peaks of the characteristic 3 peaked EPR spectra (Fig. 8b) was taken at 0, 20, 40 and 60 minutes of irradiation through a mercury UV lamp (λ_{max} = 254 nm). The blank value (PSS and spin-trap alone) was subtracted. For the colloidal nanosol samples, the value of blank in presence of HCl 0.01 M was subtracted in order to simulate the pH of TiO_2 suspensions. All the samples were analysed three times and the values were obtained by averaging these measurements. In order to make a comparison of the reactivity of the different samples, the EPR signal intensity was plotted as a function of nanoparticles concentration at 60 minutes UV irradiation time, normalizing all the data to the TiO_2 content, and reporting the slope of the relative curves.

The typical EPR parameters used were as follows: microwave frequency 9.3–9.55 Hz, microwave power 20 MW, modulation frequency 100 kHz, modulation amplitude 1500 Mg, center field 3365 G, sweep width 50 G, sweep time 30 s and number of passes 133.

Cellular oxidative stress

The ability of the samples to induce ROS production in an acellular system was tested using the DCFH assay in both murine RAW 264.7 macrophages and human A549 epithelial cells (ATCC, LGC Standards, UK). The cells were sub-cultured in RPMI 1640 Medium (Lonza, UK), supplemented with 10% heat inactivated foetal bovine serum (Gibco, UK), penicillin/streptomycin (100 U mL^{-1}; 100 μg mL^{-1}) and 2 mM L-glutamine (Sigma, Poole, UK).

Contrary to the gathered EPR data, the DCFH assay is performed in cell culture medium which contains some antioxidants. The membrane permeable dichlorodihydrofluorescein diacetate (DCFH-DA) probe was used to measure the ability of materials to induce oxidative stress in cells. After internalization, intracellular esterases cleave the diacetate moiety, thus causing probe retention and making it sensitive to ROS. DCFH was determined fluorometrically in cell lysates according to a previously described procedure,[38,39] with minor modifications. Cells were seeded in 96-well plates and treated for 24 h with RPMI cell culture medium with or without the tested materials at concentrations of 10, 20 and 40 μg cm^{-2}. These sub-lethal concentrations were selected based on dose–response (2.5–80 μg cm^{-2}) cytotoxicity analysis using the AlamarBlue® (Invitrogen, UK) and lactate dehydrogenase (Roche Diagnostics Ltd., Burgess Hill, UK) assays (data not shown). After being washed twice in sodium chloride (0.9%), cells were incubated for 1 h at room temperature in a solution of DCFH-DA (10 μM in sodium chloride) to allow internalization of the probe into the cell cytoplasm. Cells were then washed with sodium chloride and lysed in 90% DMSO in PBS. Plates were centrifuged at 300*g* for 15 min to remove cellular debris and particulates. The fluorescence was measured in the supernatants (λ_{ex} 485 nm; λ_{em} 530 nm) using a plate reader (Fluostar Optima, BMG Labtech, Aylesbury, UK). Results were expressed as change in relative fluorescence units (RFU) compared to untreated control. Using the same procedure, cells were prepared without the probe to check the material interference.

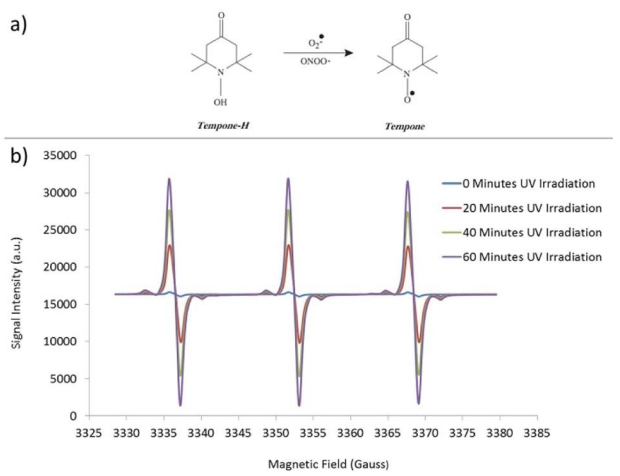

Fig. 8 (a) Use of Tempone-H as a spin trap to detect superoxide free radicals and (b) representative EPR spectrum.

Conclusions

The influence of different TiO_2 surface coatings and agglomeration state on ROS production was investigated using an acellular (EPR) and cellular assay (DCFH assay). The data of EPR analysis showed that silica coating increased the amount of ROS generated, proportionally to the amount of silica added. This trend was verified both for liquid samples in form of colloidal suspensions and for powdered samples achieved after spray drying processing. These findings likely derive from the ability of the silica layer to hinder radicals' recombination with the development of H_2O_2, so causing the accumulation of by-products $O_2^{\bullet -}$ and ·OH. The spray drying process provided an important action in terms of ROS mitigation, in fact the spray dried samples showed lower levels of ROS production as compared to the colloidal suspensions which was observed both for TiO_2 and for TiO_2–SiO_2 samples. Despite the antioxidant property of citrate, the citrate coating only caused a slight improvement in ROS production compared to uncoated TiO_2, although the increase was minor compared to the silica effect.

In vitro assessment of oxidative stress in alveolar epithelial cells and macrophages showed a decrease of ROS in the silica-

added samples, but in contrast a ROS increasing detected on all the spray dried samples. The trends found in acellular tests are, however, different from those in DCFH-DA cellular assay, due to the absence of any photo-excitation in the cellular assay. Otherwise in cells exposed to silica modified NPs, it was detected a slight decrease of oxidative stress even if no significant relationships between surface modifiers and the DCFH response could be detected. More generally, the modified forms did not attenuate the modest oxidative stress elicited by the pristine material *in vitro* cellular assay. This is significant from a SbD approach that shows that modifying pristine titania by silica can actually enhance photocatalytic activity without any significant deterioration of its biological impact.

Conflicts of interest

There are no conflicts to declare.

Acknowledgements

This research received support from the FP7 EU SANOWORK (Safe Nano Worker Exposure Scenarios) Collaborative Project (NMP4-SL-2012-280716).

Notes and references

1 Y. Ju-Nam and J. R. Lead, *Sci. Total Environ.*, 2008, **400**, 396–414.
2 N. Li, T. Xia and A. E. Nel, *Free Radical Biol. Med.*, 2008, **44**, 1689–1699.
3 V. Stone, H. Johnston and M. J. D. Clift, *IEEE Trans. Nanobioscience*, 2007, **6**, 331–340.
4 H. J. Johnston, G. Hutchison, F. M. Christensen, S. Peters, S. Hankin and V. Stone, *Crit. Rev. Toxicol.*, 2010, **40**, 328–346.
5 T. Syed, *Electrically Active Materials for Medical Devices*, Imperial College Press, New Jersey, 1 edn, 2016.
6 S. A. M. Tofail and J. Bauer, *Adv. Mater.*, 2016, **28**, 5470–5484.
7 R. Kaegi, A. Ulrich, B. Sinnet, R. Vonbank, A. Wichser, S. Zuleeg, H. Simmler, S. Brunner, H. Vonmont, M. Burkhardt and M. Boller, *Environ. Pollut.*, 2008, **156**, 233–239.
8 J. Lee, S. Mahendra and P. J. J. Alvarez, *ACS Nano*, 2010, **4**, 3580–3590.
9 X. Chen and S. S. Mao, *Chem. Rev.*, 2007, **107**, 2891–2959.
10 G. Li, S. Ciston, Z. Saponjic, L. Chen, N. Dimitrijevic, T. Rajh and K. Gray, *J. Catal.*, 2008, **253**, 105–110.
11 Z. Barbieriková, M. Mihalíková and V. Brezová, *Photochem. Photobiol.*, 2012, **88**, 1442–1454.
12 A. Nel, *Science*, 2006, **311**, 622–627.
13 R. Hjorth, L. van Hove and F. Wickson, *Nanotoxicology*, 2017, **11**, 305–312.
14 M. Valko, D. Leibfritz, J. Moncol, M. T. D. Cronin, M. Mazur and J. Telser, *Int. J. Biochem. Cell Biol.*, 2007, **39**, 44–84.
15 L. Reijnders, *Polym. Degrad. Stab.*, 2009, **94**, 873–876.
16 S. George, H. Gardner, E. K. Seng, H. Chang, C. Wang, C. H. Yu Fang, M. Richards, S. Valiyaveettil and W. K. Chan, *Environ. Sci. Technol.*, 2014, **48**, 6374–6382.
17 G. Janer, E. Mas del Molino, E. Fernández-Rosas, A. Fernández and S. Vázquez-Campos, *Toxicol. Lett.*, 2014, **228**, 103–110.
18 N. von Moos, V. B. Koman, C. Santschi, O. J. F. Martin, L. Maurizi, A. Jayaprakash, P. Bowen and V. I. Slaveykova, *RSC Adv.*, 2016, **6**, 115271–115283.
19 P. Verlooy, A. Aerts, O. I. Lebedev, G. Van Tendeloo, C. Kirschhock and J. A. Martens, *Chem. Commun.*, 2009, 4287.
20 S. P. Hudson, R. F. Padera, R. Langer and D. S. Kohane, *Biomaterials*, 2008, **29**, 4045–4055.
21 J.-H. Park, L. Gu, G. von Maltzahn, E. Ruoslahti, S. N. Bhatia and M. J. Sailor, *Nat. Mater.*, 2009, **8**, 331–336.
22 C. T. Kresge, M. E. Leonowicz, W. J. Roth, J. C. Vartuli and J. S. Beck, *Nature*, 1992, **359**, 710–712.
23 S. Ortelli, C. A. Poland, G. Baldi and A. L. Costa, *Environ. Sci.: Nano*, 2016, **3**, 602–610.
24 A. A. Torrano, Â. S. Pereira, O. N. Oliveira and A. Barros-Timmons, *Colloids Surf., B*, 2013, **108**, 120–126.
25 J. I. Kwak, W.-M. Lee, S. W. Kim and Y.-J. An, *J. Appl. Toxicol.*, 2014, **34**, 1145–1154.
26 V. Mangini, M. Dell'Aglio, A. D. Stradis, A. D. Giacomo, O. D. Pascale, G. Natile and F. Arnesano, *Chem.–Eur. J.*, 2014, **20**, 10745–10751.
27 Environmental Health Perspectives – Efficacy of Simple Short-Term *In Vitro* Assays for Predicting the Potential of Metal Oxide Nanoparticles to Cause Pulmonary Inflammation, https://ehp.niehs.nih.gov/11811/, accessed October 3, 2017.
28 A. M. Knaapen, P. J. A. Borm, C. Albrecht and R. P. F. Schins, *Int. J. Cancer*, 2004, **109**, 799–809.
29 A. A. Shvedova, A. Pietroiusti, B. Fadeel and V. E. Kagan, *Toxicol. Appl. Pharmacol.*, 2012, **261**, 121–133.
30 A. L. Costa, S. Ortelli, M. Blosi, S. Albonetti, A. Vaccari and M. Dondi, *Chem. Eng. J.*, 2013, **225**, 880–886.
31 B. M. Rotoli, O. Bussolati, A. L. Costa, M. Blosi, L. Di Cristo, P. P. Zanello, M. G. Bianchi, R. Visigalli and E. Bergamaschi, *J. Nanopart. Res.*, 2012, **14**, 1069.
32 D. K. Schwartz, *Annu. Rev. Phys. Chem.*, 2001, **52**, 107–137.
33 M. R. Miller, S. J. Borthwick, C. A. Shaw, S. G. McLean, D. McClure, N. L. Mills, R. Duffin, K. Donaldson, I. L. Megson, P. W. F. Hadoke and D. E. Newby, *Environ. Health Perspect.*, 2009, **117**, 611–616.
34 G. Bartosz, *Clin. Chim. Acta*, 2006, **368**, 53–76.
35 V. Brezová, S. Gabčová, D. Dvoranová and A. Staško, *J. Photochem. Photobiol., B*, 2005, **79**, 121–134.
36 S. Dikalov, M. Skatchkov and E. Bassenge, *Biochem. Biophys. Res. Commun.*, 1997, **230**, 54–57.
37 S. Marklund and G. Marklund, *Eur. J. Biochem.*, 1974, **47**, 469–474.
38 M. T. Siu, A. M. Shapiro, M. J. Wiley and P. G. Wells, *Toxicol. Appl. Pharmacol.*, 2013, **273**, 508–515.
39 Y. Li, X. Liu, T. Zhou, M. R. Kelley, P. Edwards, H. Gao and X. Qiao, *Redox Biol.*, 2014, **2**, 485–494.
40 Q. Wu, Z. Wang, X. Kong, X. Gu and G. Xue, *Langmuir*, 2008, **24**, 7778–7784.
41 J. Sun and L. Gao, *Carbon*, 2003, **41**, 1063–1068.

42 S. Ortelli and A. L. Costa, *Nano-Struct. Nano-Objects*, 2018, **13**, 155–162.
43 G. L. Messing, S.-C. Zhang and G. V. Jayanthi, *J. Am. Ceram. Soc.*, 1993, **76**, 2707–2726.
44 J. Oguma, Y. Kakuma, S. Murayama and Y. Nosaka, *Appl. Catal., B*, 2013, **129**, 282–286.
45 A. Kroll, C. Dierker, C. Rommel, D. Hahn, W. Wohlleben, C. Schulze-Isfort, C. Göbbert, M. Voetz, F. Hardinghaus and J. Schnekenburger, *Part. Fibre Toxicol.*, 2011, **8**, 9.
46 J. L. Kang, C. Moon, H. S. Lee, H. W. Lee, E.-M. Park, H. S. Kim and V. Castranova, *J. Toxicol. Environ. Health, Part A*, 2008, **71**, 478–485.
47 T. A. J. Kuhlbusch, A. C. John and U. Quass, *Biomarkers*, 2009, **14**, 23–28.
48 B. Ekstrand-Hammarström, C. M. Akfur, P. O. Andersson, C. Lejon, L. Österlund and A. Bucht, *Nanotoxicology*, 2012, **6**, 623–634.
49 H. Yang, Q. Wu, M. Tang, L. Kong and Z. Lu, *J. Biomed. Nanotechnol.*, 2009, **5**, 528–535.
50 S. K. Sohaebuddin, P. T. Thevenot, D. Baker, J. W. Eaton and L. Tang, *Part. Fibre Toxicol.*, 2010, **7**, 22.
51 W. Lin, Y. Huang, X.-D. Zhou and Y. Ma, *Toxicol. Appl. Pharmacol.*, 2006, **217**, 252–259.
52 M. J. Akhtar, M. Ahamed, S. Kumar, H. Siddiqui, G. Patil, M. Ashquin and I. Ahmad, *Toxicology*, 2010, **276**, 95–102.